

RESEARCH ARTICLE

Quantification of Dynamic [^{18}F]FDG Pet Studies in Acute Lung Injury

Elisabetta Grecchi,^{1,6} Mattia Veronese,^{2,6} Rosa Maria Moresco,³ Giacomo Bellani,^{4,5} Antonio Pesenti,^{4,5} Cristina Messa,³ Alessandra Bertoldo⁶

¹Division of Imaging Science and Biomedical Engineering, King's College London, London, UK

²Department of Neuroimaging, Institute of Psychiatry, Psychology & Neuroscience, King's College London, London, UK

³Tecnomed Foundation, University of Milan-Bicocca, Milan, Italy

⁴Department of Health Science, University of Milan-Bicocca, Monza, Italy

⁵Department of Emergency and Intensive Care, San Gerardo Hospital, Monza, Italy

⁶Department of Information Engineering (DEI), University of Padova, Via G. Gradenigo 6/B, 35131, Padova, Italy

Abstract

Purpose: This work aims to investigate lung glucose metabolism using 2-deoxy-2- ^{18}F fluoro-D-glucose (^{18}F]FDG) positron emission tomography (PET) imaging in acute lung injury (ALI) patients.

Procedures: Eleven ALI patients and five healthy controls underwent a dynamic ^{18}F]FDG PET/X-ray computed tomography (CT) scan. The standardized uptake values (SUV) and three different methods for the quantification of glucose metabolism (*i.e.*, ratio, Patlak, and spectral analysis iterative filter, SAIF) were applied both at the region and the voxel levels.

Results: SUV reported a lower correlation than the ratio with the net tracer uptake. Patlak and SAIF analyses did not show any significant spatial or quantitative ($R^2 > 0.80$) difference. The additional information provided by SAIF showed that in lung inflammation, elevated tracer uptake is coupled with abnormal tracer exchanges within and between lung tissue compartments.

Conclusions: Full kinetic modeling provides a multi-parametric description of glucose metabolism in the lungs. This allows characterizing the spatial distribution of lung inflammation as well as returning the functional state of the tissues.

Key words: Acute lung injury, ^{18}F]FDG, Positron emission tomography, Spectral analysis, Parametric imaging

Introduction

Pulmonary inflammatory pathologies, such as acute lung injury (ALI) and acute respiratory distress syndrome (ARDS), are severe forms of respiratory failures that affect

approximately 80 per 100,000 person-years with a mortality rate of 25–40 % [1–3]. These diseases are characterized by a diffusive neutrophil alveolar infiltration [4], which is associated with an increased cellular metabolism and glucose consumption. Positron emission tomography (PET) imaging with the glucose analog 2-deoxy-2- ^{18}F fluoro-D-glucose (^{18}F]FDG) is widely used to assess *in vivo* tissue metabolism [5]. Therefore, ^{18}F]FDG PET imaging is a valuable tool to study lung inflammation *in vivo* [6, 7] because it allows measuring the level of inflammation and its distribution in the tissues [8, 9].

Electronic supplementary material The online version of this article (doi:10.1007/s11307-015-0871-3) contains supplementary material, which is available to authorized users.

Correspondence to: Alessandra Bertoldo; e-mail: bertoldo@dei.unipd.it

A single static PET image minimizes the discomfort when scanning fragile populations, such as ALI patients [9]. However, quantification can only be performed by measuring the standardized uptake value (SUV) [9]. SUV is a simple and straightforward index of tracer uptake, but it introduces quantification bias since it is neither directly linked to any physiological process nor independent on blood flow and blood-to-tissue tracer transportation [10].

By contrast, dynamic PET studies offer the possibility of full kinetic modeling. Kinetic modeling allows a quantitative description of tracer behavior by taking into account the blood flow and the transportation rate constants between the blood and the tissue [11], which is particularly important in lung studies. For instance, the fraction of blood volume is significantly higher in the lungs compared to other tissues [12, 13], and its exclusion from the quantification model might bias the results when analyzing data both at the region of interest (ROI) and the voxel levels [14]. Moreover, the increased permeability of the capillary membrane due to ALI/ARDS may cause alveolar flooding, infiltration by neutrophils and macrophages, and formation of hyaline membranes. By consequence, the physiological equilibrium between the pulmonary interstitium and the capillary vessels, and the resulting tracer kinetics, can be altered. Information about capillary–tissue exchanges might be of interest for disease characterization and classification.

Despite these potential advantages, fully quantitative [^{18}F]FDG PET studies for lung tissues have been limited mostly to animal models [15–17]. These studies demonstrated that parameters derived from a dynamic scan allow more accurate disease classification and support therapy assessment [4, 17]. In humans, dynamic [^{18}F]FDG PET studies and a Patlak graphical analysis allowed a subclassification of ALI patients on the basis of the characteristics of tracer uptake in normal and pathological lung tissues [18, 19]. The graphical Patlak analysis, both at the ROI and the voxel levels, does not require *a priori* definition of any kinetic model, but it assumes that the tracer is irreversibly trapped into the tissue and the blood volume is negligible [19]. Because this assumption might be inappropriate for lung tissues, a specific quantitative approach for [^{18}F]FDG dynamic PET studies in the human lungs is needed.

In this work, we tested several approaches, in particular spectral-based methodologies, for the quantification of dynamic [^{18}F]FDG PET data in the human lungs. Differences in glucose metabolism and transportation from the blood to the alveolar space in normal and inflamed lungs were studied by comparing healthy volunteers and ALI patients.

Materials and Methods

Subjects

Five normal subjects (68.8 kg \pm 6.5 kg) and 11 ALI patients (75.2 kg \pm 10.7 kg) were recruited from the general intensive care unit (ICU) of San Gerardo Hospital in Monza, Italy. The protocol is fully described in [18].

Before imaging, hemodynamic and ventilation variables were measured while the patient was on volume-controlled ventilation. Expiratory and inspiratory pauses were performed to measure the positive end-expiratory pressure (PEEP) and the plateau pressure (Pplat). Respiratory system compliance (Crs) was computed as $Crs = VT / (Pplat - PEEP_{tot})$, where VT is the tidal volume. An intensive care ventilator was used for all patients. The invasive arterial blood pressure, electrocardiogram, peripheral oxygen saturation, and expired CO₂ were monitored continuously. Ventilation settings, sedation, and fluid therapy were maintained constant throughout the study unless clinically advised.

Image Acquisition

All subjects underwent a dynamic PET/CT [^{18}F]FDG scan performed with a GE Discovery ST equipped with an eight-slice CT (GE Healthcare, Milwaukee, WI). The GE Discovery ST has an axial field of view of approximately 18 cm. The spiral CT scan acquisitions were performed while the subject was in apnea, and the mean airway pressure was kept at the same level as during mechanical ventilation (by switching the ventilator to constant positive airway pressure modality). This was done to ensure the best possible coregistration between the CT and the PET acquisition, performed afterwards during tidal ventilation. PET acquisition started 5 s after tracer injection (\sim 300 MBq of [^{18}F]FDG) and consisted of 12 frames of 10 s each ($12 \times 10''$), followed by $10 \times 30''$, $8 \times 300''$, and $1 \times 600''$, for a total imaging time of 57 min.

Image Processing

Dynamic PET data were reconstructed with OSEM iterative algorithm and corrected for decay, and scatter and random counts. The CT images were used to manually outline ROIs comprising the whole lungs and two subregions within the lungs, corresponding to the normally ventilated areas (“aerated ROIs”) and hyperdense areas (“collapsed ROIs”). The aerated ROIs were drawn over voxels whose CT attenuation was comprised of between -100 and $+100$ Hounsfield units and the collapsed ROIs over voxels between -900 and -501 Hounsfield units [18].

The individual arterial input function was derived directly from the PET images of each subject by manually drawing a ROI in the center of the descending aorta [20]. The plasma fraction over the blood image-derived activity was calculated assuming a constant partition coefficient of 1.136. This number was derived by Cobelli’s formula [21] assuming a lung hematocrit of 40 %. The analysis was performed by expert trained clinicians.

Quantification

The [^{18}F]FDG fractional metabolic rate K_i (ml/cm³/min) was calculated both at the ROI and the voxel levels using four quantification methods: the spectral analysis iterative filter (SAIF) [22], the Patlak analysis [23], the ratio method [24], and the standardized uptake value (SUV, g/ml) [25]. These methods are described in detail in the [supplementary materials](#) (refer to the Quantification Methods section). Notably, while SAIF and Patlak require a full dynamic acquisition, only three and one static images

are necessary for the ratio method and SUV, respectively. However, only SAIF and Patlak allow the absolute quantification of K_i (hereafter referred to as $K_{i, \text{SAIF}}$ with $K_{i, \text{Patlak}}$), as the ratio method and SUV provide only a semiquantitative value of tissue tracer uptake.

K_i was chosen as the reference parameter for comparison, as it is the only one with an explicit physiological meaning (values derived from the ratio method and the SUV are just approximations of the real [^{18}F]FDG metabolic rate).

Model Development

Compared to static scans, dynamic scans analyzed with spectral-based methods reveal additional information on the underlying physiopathological process that influences [^{18}F]FDG uptake. These additional parameters might be potential biomarkers for ALI. To achieve this goal, the number of kinetic components necessary to describe the tracer behavior in lung tissue has to be determined. Therefore, a full analysis with SAIF in both healthy subjects and patients was performed. In addition to anatomical defined ROIs, clustering analysis was performed to segment the lung in functionally homogeneous ROIs, to confirm that the findings were not due to tissue heterogeneity or noise in the data. A *k-means* clustering, based on the voxels kinetics, was performed within each ROI (delineated from the Hounsfield units—see above) to obtain six functionally homogeneous clusters [26].

Once the number of components necessary to describe the system was determined, all voxels were re-analyzed with a non-linear spectral analysis [27]. The non-linear SA is similar to the linear SA [28, 29], but the number of components must be fixed *a priori*, resulting in a more stable and robust solution to the model. To note that for voxel-wise estimation the noise level is higher than the ROIs' and that might lead to a different degree of accuracy in the quantification [30].

Parametric Imaging

The voxel-wise application of non-linear SA analysis returns parametric maps for K_i (glucose uptake rate, $\text{ml}/\text{cm}^3/\text{min}$), K_1 (tracer transport rate from plasma to tissue, $\text{ml}/\text{cm}^3/\text{min}$), and V_b (vascular fraction in the observed volume, unitless). In addition, for each of the model kinetic components, a distribution volume V_i (ml/cm^3) can be computed [11, 31]. Since normalization in a standard reference space is not possible for lung imaging, a region-based comparison of these maps was performed between groups. The mean of voxel estimates within ROIs was considered for each subject. Outliers (corresponding to negative or unreliable estimates) were discarded from the analysis.

Results

Method Comparison

Correlation analyses were performed using healthy volunteers and ALI patients together, because the performance of a given methodology is not likely to depend on the subject's condition.

At the region level, $K_{i, \text{Patlak}}$, ratio, and SUV significantly correlated with $K_{i, \text{SAIF}}$ (Fig. 1). As expected, the highest correlation was between $K_{i, \text{SAIF}}$ and $K_{i, \text{Patlak}}$, because they are direct estimations of the same physiological index. The correlation of the semi-static (ratio) method with $K_{i, \text{SAIF}}$ was less good and that of the static method (SUV) even less (Fig. 1), which suggests that at least some dynamic information is preferable to describe the tracer behavior.

Similar results were found at the voxel level. Pearson's correlation coefficients R^2 were the following: 0.80 ($K_{i, \text{SAIF}}-K_{i, \text{Patlak}}$), 0.60 ($K_{i, \text{SAIF}}-\text{ratio}$), and 0.37 ($K_{i, \text{SAIF}}-\text{SUV}$). Examples of parametric maps are shown in Fig. 2.

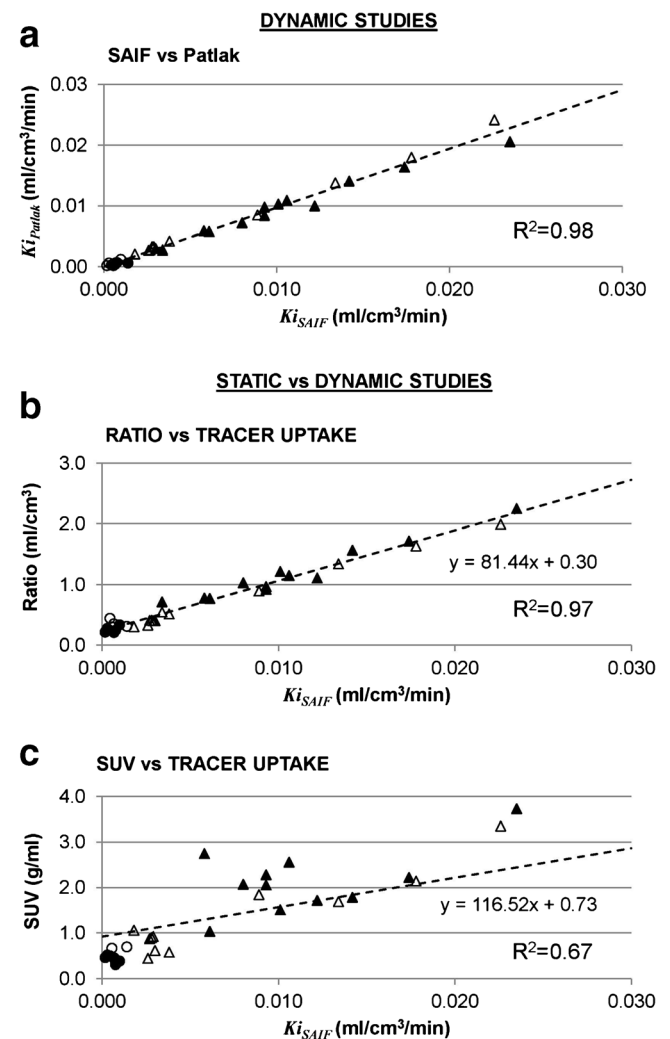


Fig. 1 Correlation analysis of $K_{i, \text{Patlak}}$, ratio, and SUV estimates with $K_{i, \text{SAIF}}$ at the ROI level. The circles represent the uptake estimates in normal (black) and hyperdense-collapsed (open) ROIs for all the healthy subjects while the triangles represent the uptake estimates in normal (black) and hyperdense-collapsed (open) ROIs for all the ALI patients. The dashed line represents the regression line. **a** $K_{i, \text{SAIF}}-K_{i, \text{Patlak}}$ correlation; **b** $K_{i, \text{SAIF}}-\text{ratio}$ correlation; **c** $K_{i, \text{SAIF}}-\text{SUV}$ correlation.

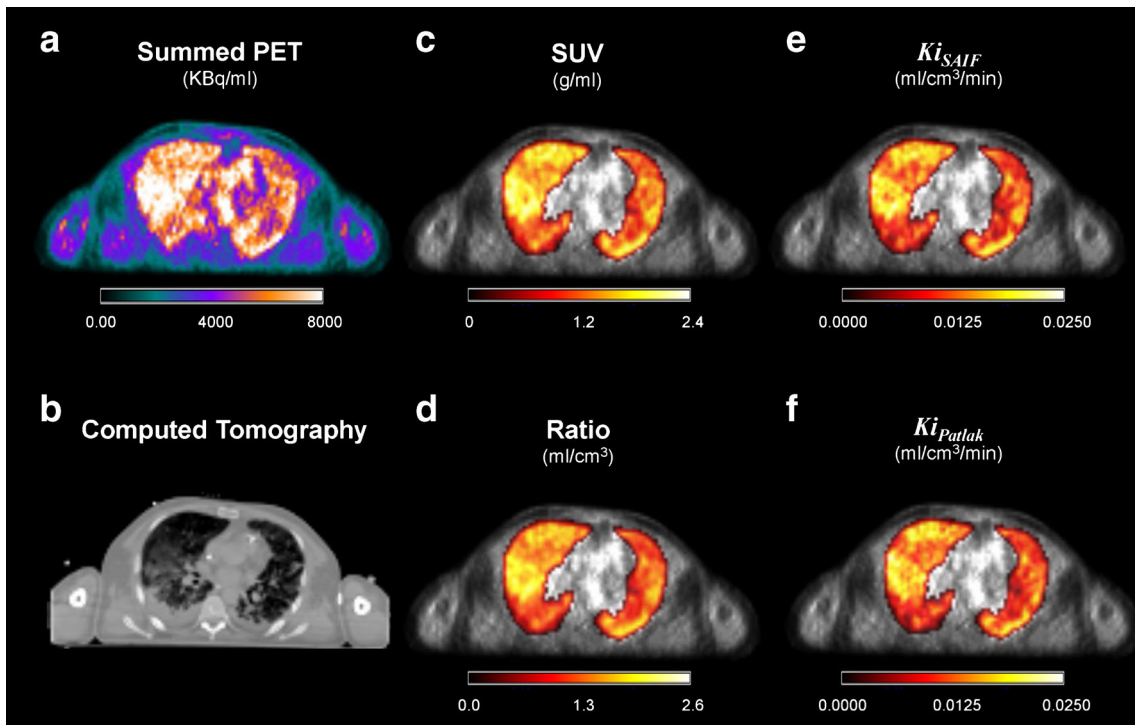


Fig. 2 Visual comparison of parametric maps in a representative healthy subject: **a** summed PET image; **b** CT; **c** SUV; **d** ratio; **e** Ki_{SAIF} ; **f** Ki_{Patlak} . Please note that, although the overall aspect of the maps is similar with the four methods, the maps obtained with SAIF and Patlak are sharper and have better defined boundaries of the “hot” areas.

Derivation of Additional Physiological and Pathophysiological Information

All spectra found after anatomical segmentation, in both healthy volunteers and ALI patients, displayed a trapping component (*i.e.*, line corresponding to $\beta=0$) and two equilibrating components (*i.e.*, lines corresponding to $\beta \neq 0$): a slower one close to the trapping and a faster one close to the plasma compartment (Fig. 3). These components are likely to represent, respectively, the overall [^{18}F]FDG kinetic in tissue (the trapping component) and the tracer exchanges between the plasma and the tissue and within the tissue (the two equilibrating components).

The estimated number of spectral lines did not change between healthy subjects and patients and between normal and hyperdense lung regions (Fig. 3). ALI patients had, however, a higher trapping component and the shift of the second kinetic component towards higher β values (Fig. 3).

The results were similar when SAIF was used after cluster-based functional segmentation at the ROI level (Supplementary Material—Figure 1). Indeed, 93 % (in healthy subjects) and 95 % (in ALI patients) of the clusters showed a spectrum with two equilibrating components and a trapping component (after anatomical segmentation, the percentages were 90 and 100 % for healthy volunteers and ALI patients, respectively).

These results were supported by the voxel-wise analysis, as 49 % (in healthy subjects) and 53 % (in ALI patients) of the voxels showed a similar spectrum, despite the higher

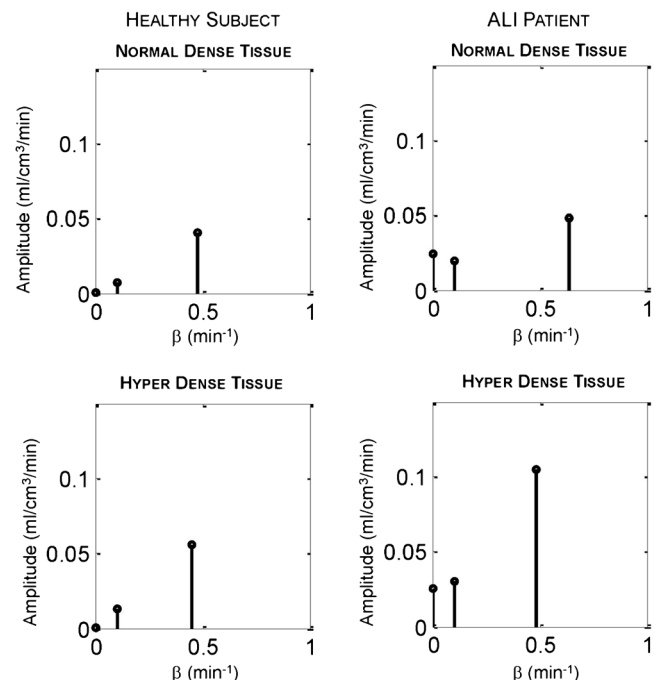


Fig. 3 Examples of kinetic spectra derived from SAIF quantification of normal and hyperdense-collapsed tissue in one representative healthy subject and one patient. Hyperdense tissue in the healthy control is reported for comparative purposes, since it represents less than 1 % of the entire lung tissue.

noise level that is intrinsic to any analysis at the voxel level. In light of these results, a two exponential model was chosen and all subjects were re-analyzed by non-linear SA. This allowed defining V1 and V2 as the volume of distribution of the slowest and the fastest kinetic component, respectively. A summary of these estimates is reported in Table 1.

Notably, despite the use of a different estimator and of different modeling assumptions, linear and non-linear SA returned the same K_i estimates (Supplementary Material—Figure 2). On the other hand, the parameter estimation using non-linear SA yielded a considerable amount of outliers (21–57 %). These outliers are expected because non-linear estimators are more sensitive to noise compared to the linear one. Indeed, the number of outliers was smaller in the patients group, where the PET signal is stronger due to inflammation, and hence, the noise level is lower.

Group Comparison

ALI patients generally showed higher values in all parameters (K_i , K1, V1, and V2) than healthy subjects (Fig. 4). In particular, K_i was significantly different ($p < 0.05$) between the two groups (Fig. 4a).

Among the ALI patients, it is possible to discriminate two subgroups based on the tracer uptake comparison between tissue types. Compared to healthy subjects, one patient subgroup had a high tracer uptake in both normal and hyperdense tissues (group A—four patients) while a second subgroup had higher values only in the hyperdense tissue (group B—seven patients). Similar results were obtained when the same analysis was performed with SUV or ratio quantifications (Supplementary materials—Figure 4). A detailed description of different estimates for each subgroup is reported in Table 2.

This classification is consistent with patient clinical conditions and in agreement with the findings reported by Bellani *et al.* [18]. ALI patients belonging to group A had a more severe impairment of gas exchanges and

mechanical properties of the respiratory system than those of group B. In fact, group A patients had a lower ratio between partial arterial pressure of oxygen and inspired oxygen fraction ($\text{PaO}_2/\text{FiO}_2$, 125.26 vs. 190.42 mmHg, $p < 0.05$) despite a higher PEEP (13.0 ± 1.1 vs. 10.3 ± 1.4 cmH₂O, $p < 0.05$) and a lower compliance (27.5 ± 7.7 vs. 50.3 ± 10.2 ml/cmH₂O, $p < 0.01$).

In addition to the tracer trapping rate, these two subgroups could be discriminated on the basis of the value of K1 ($p < 0.05$). Also, in ALI subgroup B, both K_i and K1 were significantly different between normal and hyperdense tissues. Similarly, V1 and V2 differed between healthy subjects and ALI patients and between normal and hyperdense tissue, even if differences of V2 were not statistically significant.

The pattern of spatial distribution of the parameters can be qualitatively observed in the maps reported in Fig. 5. All parameters were higher in patients compared to healthy controls, except for Vb. Notably, in ALI patients, K1, V2, and Vb had different spatial distribution maps from K_i and V1. A quantitative evaluation of differences between parameter estimates of patients belonging to different groups can be seen in Fig. 6. Overall, both volumes of distributions were higher in group A. The volume of distribution of the slowest compartment (V1) gradually increased along with CT density in both ALI groups. Similarly, the fastest compartment (V2) increased with CT density in the patients of group A, but no significant change was observed in the patients of group B.

Discussion

Considerations on Study Findings

The primary aim of this study was to compare different quantification approaches for dynamic [¹⁸F]FDG PET data in human lungs and evaluate their potential for patient clinical evaluation. Typically, in a [¹⁸F]FDG PET study,

Table 1. Non-linear spectral analysis estimates

	K_i	K1	Vb	V1	V2	K_i	K1	Vb	V1	V2
Healthy ^a (5 subjects)	Hyperdense-collapsed tissue					Normal tissue				
Mean	0.0014	0.18	0.08	0.10	0.023	0.0017	0.21	0.12	0.15	0.030
SD	0.0003	0.11	0.04	0.03	0.010	0.0004	0.13	0.06	0.06	0.021
Min	0.0010	0.08	0.02	0.08	0.013	0.0013	0.08	0.05	0.11	0.003
Max	0.0018	0.35	0.11	0.14	0.038	0.0023	0.40	0.19	0.24	0.062
All patients ^b (11 patients)	Hyperdense-collapsed tissue					Normal tissue				
Mean	0.0082	0.17	0.04	0.16	0.027	0.0127	0.22	0.06	0.32	0.045
SD	0.0074	0.05	0.02	0.06	0.011	0.0054	0.08	0.03	0.11	0.024
Min	0.0024	0.07	0.01	0.08	0.014	0.0087	0.13	0.01	0.17	0.024
Max	0.0239	0.23	0.08	0.27	0.048	0.515	0.36	0.12	0.49	0.091

SD, min, and max refer to the standard deviation and the minimum and maximum regional estimates (as calculated from the mean voxel distribution) across subjects

$K1$ transport rate from plasma to tissues (ml/cm³/min), Vb blood volume (unitless), $V1$ volume of distribution in the fastest compartment (ml/cm³), $V2$ volume of distribution in the slowest compartment (ml/cm³)

^aMeans of voxel estimates within regions computed for the healthy subject group

^bMeans of voxel estimates within regions computed for all the ALI patients

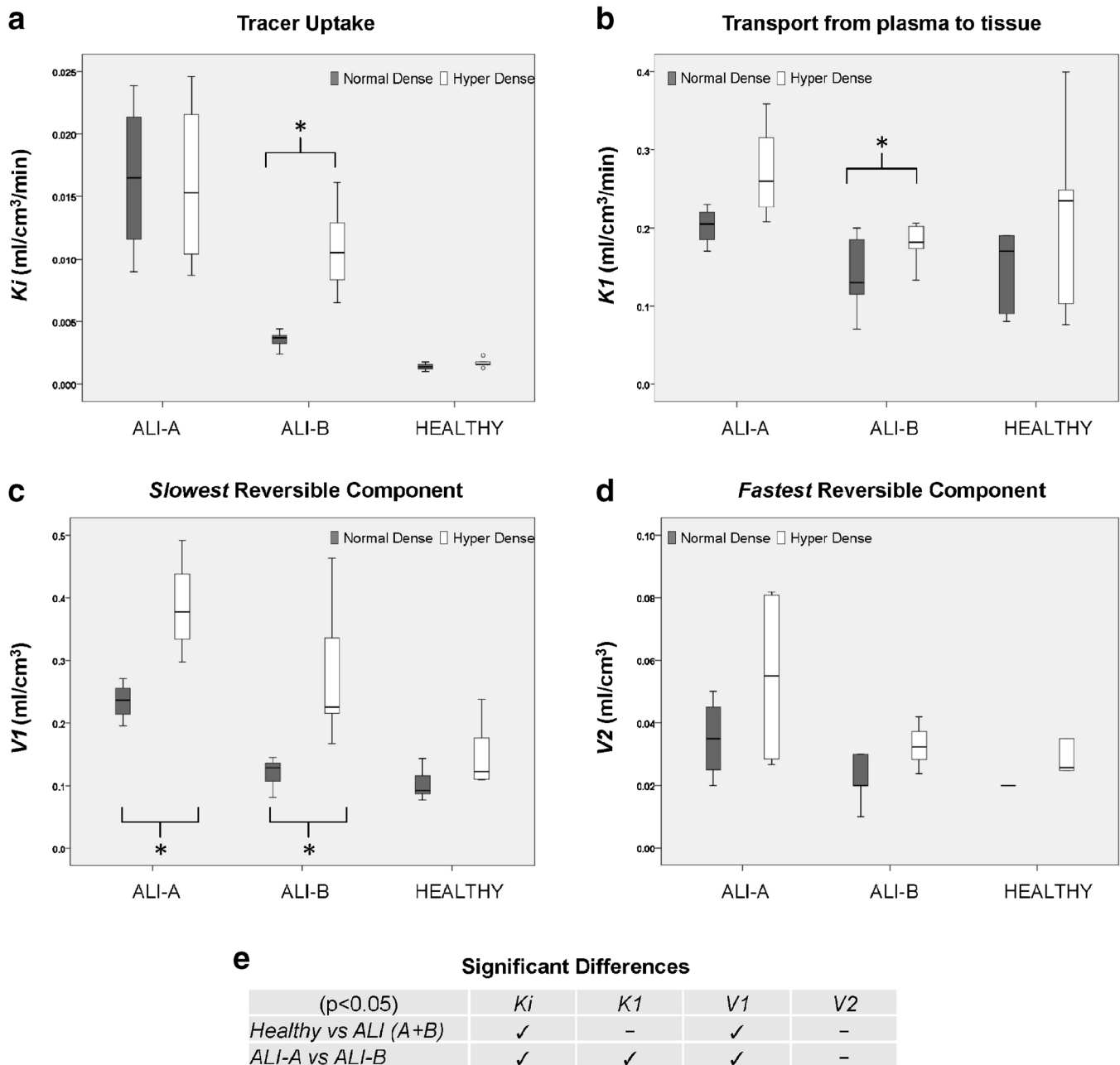


Fig. 4 Parameter estimates and statistics obtained with non-linear SAIF in the whole dataset (five healthy controls, four ALI-A and seven ALI-B patients). Grey bars normal tissue, white bars hyperdense-collapsed tissue. ALI patients are divided into two subgroups according to the K_i values. For each bar, the mean and standard deviation are reported. The stars (*) indicate statistical significance ($p < 0.05$; t test) between hyperdense and normal tissues within a given group of subjects. **a** Net tracer uptake K_i ; **b** transport rate from plasma to tissue K_1 ; **c** volume of distribution in the fastest compartment V_1 ; **d** volume of distribution in the slowest compartment V_2 ; **e** Statistical significance ($p < 0.05$; t test) between the different groups.

the accumulation of the tracer in the tissues (K_i) is used as proxy of the [^{18}F]FDG metabolism. The correlation analysis between $K_{i, \text{SAIF}}$, $K_{i, \text{Patlak}}$, and semiquantitative indices suggests that while the ratio method might be a valid alternative to the full dynamic analysis, the SUV might not be ($R^2 K_{i, \text{SAIF vs. SUV}} = 0.68$ region-wise, 0.37 voxel-wise). This is in agreement with previous studies showing that the ratio method better describes the tracer kinetic than SUV [32, 33].

Despite the good correlation between $K_{i, \text{SAIF}}$ and $K_{i, \text{Patlak}}$, the full quantitative analysis obtained with SAIF provides additional kinetic information, which would not be otherwise available.

First, spectral-based methods, *i.e.*, SAIF and non-linear SA, showed that the optimal model for [^{18}F]FDG kinetic in lung tissue, both normal and inflamed, is described by two exponential components and one trapping component. These components represent, respectively, the reversible exchanges

Table 2. Estimates summary

	SUV	Ratio	K_i	K1	Vb	V1	V2	SUV	Ratio	K_i	K1	Vb	V1	V2
Healthy ^a (5 subjects)								Normal tissue						
Mean	0.601	0.358	0.0014	0.18	0.08	0.10	0.023	0.422	0.256	0.0017	0.21	0.12	0.15	0.030
SD	0.120	0.059	0.0003	0.11	0.04	0.03	0.010	0.077	0.052	0.0004	0.13	0.06	0.06	0.021
Min	0.448	0.300	0.0010	0.08	0.02	0.08	0.013	0.311	0.209	0.0013	0.08	0.05	0.11	0.003
Max	0.120	0.444	0.0018	0.35	0.11	0.14	0.038	0.510	0.337	0.0023	0.40	0.19	0.24	0.062
ALI—group A ^b (4 patients)								Normal tissue						
Mean	2.38	1.544	0.0165	0.20	0.04	0.24	0.033	2.254	1.467	0.0160	0.27	0.06	0.39	0.055
SD	0.948	0.548	0.0064	0.03	0.01	0.03	0.012	0.752	0.465	0.0070	0.06	0.03	0.08	0.030
Min	1.510	1.032	0.0090	0.17	0.02	0.20	0.018	1.691	0.895	0.0087	0.21	0.04	0.30	0.027
Max	3.727	2.251	0.0239	0.23	0.06	0.27	0.048	3.348	1.992	0.0246	0.36	0.10	0.49	0.082
ALI—group B ^c (7 patients)								Normal tissue						
Mean	2.745	1.027	0.0035	0.14	0.04	0.12	0.023	0.0108	0.768	0.396	0.20	0.06	0.28	0.040
SD	0.578	0.275	0.0007	0.05	0.02	0.02	0.006	0.0035	0.225	0.067	0.07	0.03	0.10	0.023
Min	1.031	0.770	0.0024	0.07	0.01	0.08	0.014	0.0065	0.441	0.305	0.13	0.01	0.17	0.024
Max	2.745	1.556	0.0044	0.20	0.08	0.15	0.030	0.0161	1.057	0.515	0.36	0.12	0.46	0.091

SD, min, and max refer to the standard deviation and the minimum and maximum regional estimates (as calculated from the mean voxel distribution) across subjects
 SUV/standardize uptake value (g/ml), ratio (ml/cm³), K_i net tracer uptake (ml/cm³/min), K_1 transport rate from plasma to tissues (ml/cm³/min), V_b blood volume (unitless), V_1 volume of distribution in the fastest compartment (ml/cm³), V_2 volume of distribution in the slowest compartment (ml/cm³)

^aMeans of voxel estimates within regions computed for the healthy subject group

^bMeans of voxel estimates within regions computed for the ALI patient group with a high level of tracer uptake in both normal and hyperdense tissues

^cMeans of voxel estimates within regions computed for the ALI patient group with a high level of tracer uptake, measured only in hyperdense tissues

and the irreversible accumulation of the tracer in the tissue. Although SAIF cannot unequivocally attribute each component to a specific physiological event, these results reflect the number of compartments of the model proposed by Schroeder and colleagues [15–17]. We, however, cannot validate the arrangement proposed by Schroeder *et al.* for their model, according to which the extracellular compartment is not directly connected to the plasma-cellular one (see Figure 1a of [15]). In fact, the findings of spectral analysis are compatible with multiple alternative models. Only a precise understanding of alveolar–blood exchanges would allow selecting the most appropriate model configuration of [¹⁸F]FDG kinetic in the lungs.

Second, multiple parameters, other than K_i , can be derived with spectral-based methods. These parameters provide valuable information on glucose metabolism. For instance, the analysis of K1 and Vb enables the characterization of capillary–tissue exchange integrity: K1 is linked to the magnitude of tissue inflammation and/or capillary breakage and Vb differentiates normal from abnormal capillary volumes. Notably, these two parameters do not carry the same information since their spatial distribution can be independent (see Fig. 5 where K1 is overall uniform while Vb shows a more heterogeneous distribution). Similarly, the values of V2 (*i.e.*, exchange rate between capillary and interstitium) and V1 (*i.e.*, exchange rate between interstitium and tissue) reflect the physiological conditions of the alveolar interstitium and tissue transports. When both of them are increased, the tissue is likely to be damaged and possibly associated with edema and/or capillary breakage.

Our analyses allowed us to discriminate two subgroups of patients with ALI. Interestingly, the distinction between group A and group B reflects an actual clinical condition, as patients in group A had a more severe impairment of gas exchanges and mechanical properties. Albeit indirectly, the higher V1 and V2 values in group A patients might suggest the presence of a higher endothelial–alveolar barrier permeability. Further studies are necessary to confirm this hypothesis.

Considerations on Study Limitations

This study is one of the first of its kind conducted on a human cohort. Some methodological assumptions should be also evaluated critically.

To begin with, we assumed that [¹⁸F]FDG is irreversibly trapped in the lungs. This choice was based on data reported in the literature [34–36]. Our findings support this hypothesis, given the strong linearity of the Patlak regression analyses and the fact that SAIF does not converge when applied to reversible tracers [37]. Further support is given by the traditional spectral analysis, which does not require the irreversibility assumption but still shows a trapping component in all voxels of the entire dataset (data not shown).

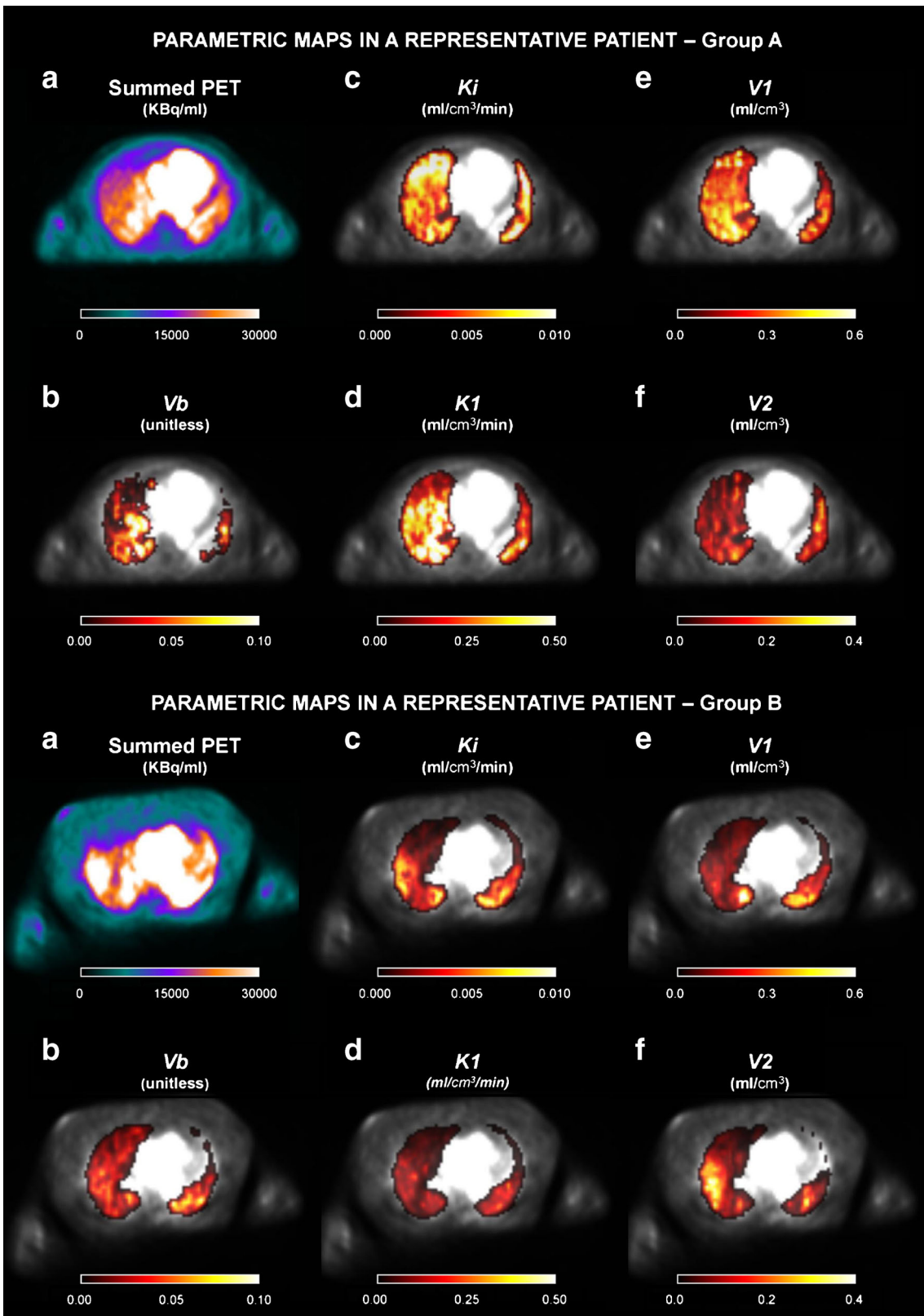


Fig. 5 Parametric maps obtained with SAIF at the voxel level for two representative patients (*upper panels* group A patient, *lower panels* group B patient). Please refer to Supplementary Material Figure 3 for maps of a healthy subject. Maps refer to a summed PET image; *b* blood volume V_b ; *c* net tracer uptake K_i ; *d* transport rate from plasma to tissue K_1 ; *e* volume of distribution V_1 ; *f* volume of distribution V_2 .

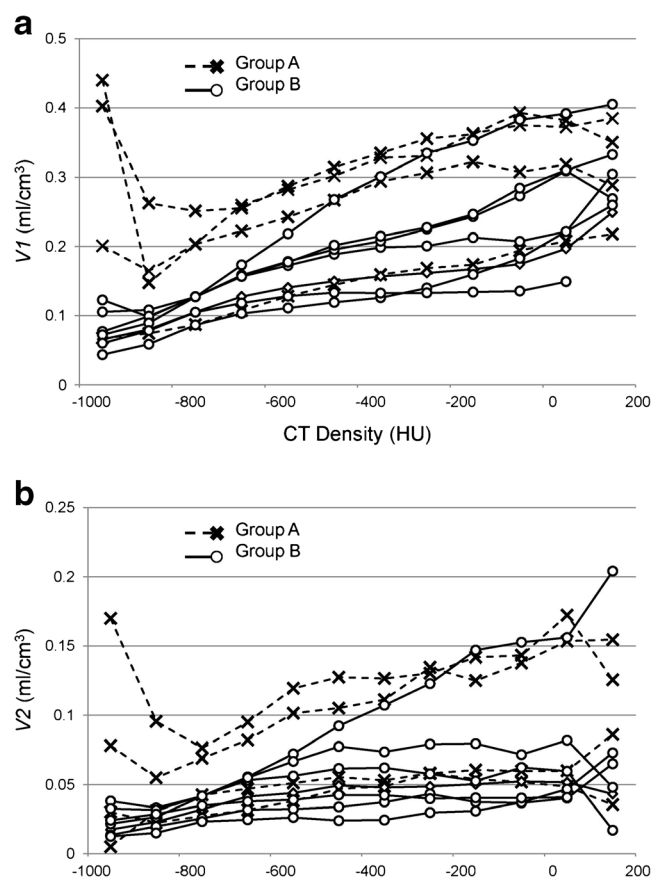


Fig. 6 Volumes of distribution mean values in 12 different ROIs for ALI patients. Twelve different ROIs are defined based on CT density. The mean values are reported for each patient (*dashed line* group A; *solid line* group B). **a** Volume of distribution in the fastest compartment V1; **b** volume of distribution in the slowest compartment V2.

In second instance, we did not perform respiratory motion correction. This is, however, an unlikely source of bias in our study. The presence of the two intermediate lines in the SAIF spectrum cannot be a consequence of patient motion, because PET data are the averaged images of multiple respiratory cycles. Furthermore, the frequencies of these two spectral lines differ of more than one order of magnitude, which makes the hypothesis of an artifact unlikely. Motion correction might, however, improve the quality of kinetic modeling and should be performed whenever possible.

Furthermore, we used an image-derived input function, rather than serial arterial sampling. First, given the diameter of the first part of the aorta, no significant partial volume effects are expected. Then, we tested our results by using a population-based input function obtained from an independent dataset [27], rescaled to account for the experimental differences between the two protocols. No significant differences were found in terms of K_i values and number of spectral components. Please note that the clinical conditions of the patients in this study were not compatible with arterial cannulation.

Finally, it is important to underline that the sample size of the dataset (5 healthy controls vs. 11 ALI patients) is a critical factor for an ultimate clinical investigation of the disease. Larger trials are necessary to confirm our preliminary findings, especially ALI subclassification.

Conclusion

Dynamic [¹⁸F]FDG PET imaging is a valuable tool to study glucose metabolism in the inflamed lung. Fully kinetic modeling with spectral-based methods provides a unique insight into the pathophysiology of ALI, allowing a better understating of the lung inflammation process and a more comprehensive description of the functional state of the tissue.

[¹⁸F]FDG kinetics in human lung tissue can be described by an exponential model with two equilibrating components and one trapping component. The parameters derived can be correlated with the severity of the disease and can identify damaged areas by evaluating tissue–capillary integrity and tracer exchange rates.

Acknowledgments. We thank Dr. Paolo Zanotti-Fregonara for providing an invaluable editorial assistance.

Conflict of Interest. The authors declare that they have no conflict of interest.

Compliance with Ethical Standards.

Funding. This study was funded in part by UK Medical Research Council (MRC): program grant “Quantitative methodologies for Positron Emission Tomography,” No. G1100809/1.

Ethical Approval. All procedures performed were in accordance with the ethical standards of the internal institution’s ethical committee and with the 1964 Helsinki declaration and its later amendments or comparable ethical standards.

This article does not contain any studies with animals performed by any of the authors.

Informed Consent. Informed consent was obtained from all individual participants for whom identifying information is included in this article according to the committee’s recommendations.

Electronic Supplementary Material

Below is the link to the electronic supplementary material. [ESM 1\(PDF 3622 kb\)](#)

References

1. Rubenfeld GD, Caldwell E, Peabody E et al (2005) Incidence and outcomes of acute lung injury. *N Engl J Med* 353:1685–1693
2. Wheeler AP, Bernard GR (2007) Acute lung injury and the acute respiratory distress syndrome: a clinical review. *Lancet* 369:1553–1564
3. Erickson SE, Martin GS, Davis JL et al (2009) Recent trends in acute lung injury mortality: 1996–2005. *Crit Care Med* 37:1574
4. de Prost N, Tucci MR, Melo MFV (2010) Assessment of lung inflammation with 18F-FDG PET during acute lung injury. *Am J Roentgenol* 195:292–300
5. Gallamini A, Zwarthoed C, Borra A (2014) Positron emission tomography (PET) in oncology. *Cancer* 6:1821–1889

6. Jones HA (2005) Inflammation imaging. *Proc Am Thorac Soc* 2:545–548
7. Schroeder T, Melo MFV, Musch G et al (2007) PET imaging of regional ¹⁸F-FDG uptake and lung function after cigarette smoke inhalation. *J Nucl Med* 48:413–419
8. Chen DL, Ferkol TW, Mintun MA et al (2006) Quantifying pulmonary inflammation in cystic fibrosis with positron emission tomography. *Am J Respir Crit Care Med* 173:1363–1369
9. Rodrigues R, Miller P, Bozza F et al (2008) FDG-PET in patients at risk for acute respiratory distress syndrome: a preliminary report. *Intensive Care Med* 34:2273–2278
10. Boellaard R (2009) Standards for PET image acquisition and quantitative data analysis. *J Nucl Med* 50:11S–20S
11. Bertoldo A, Rizzo G, Veronese M (2014) Deriving physiological information from PET images: from SUV to compartmental modelling. *Clin Transl Imaging* 2:239–251
12. Dock DS, Kraus WL, McGuire LB et al (1961) The pulmonary blood volume in man. *J Clin Invest* 40:317
13. Fishman AP (1966) The volume of blood in the lungs. *Circulation* 33:835–838
14. Schroeder T, Vidal Melo MF, Venegas JG (2011) Analysis of 2-[fluorine-18]-fluoro-2-deoxy-D-glucose uptake kinetics in PET studies of pulmonary inflammation. *Acad Radiol* 18:418–423
15. Schroeder T, Vidal Melo MF, Musch G, Harris RS et al (2008) Modeling pulmonary kinetics of 2-deoxy-2-[¹⁸F] fluoro-d-glucose during acute lung injury. *Acad Radiol* 15:763–775
16. Dittrich AS, Winkler T, Wellman T et al (2012) Modeling 18F-FDG kinetics during acute lung injury: experimental data and estimation errors. *PLoS One* 7, e47588
17. de Prost N, Feng Y, Wellman T, et al. (2014) 18F-FDG Kinetics parameters depend on the mechanism of injury in early experimental acute respiratory distress syndrome. *J Nucl medicine:jnumed*. 114.140962
18. Bellani G, Messa C, Guerra L et al (2009) Lungs of patients with acute respiratory distress syndrome show diffuse inflammation in normally aerated regions: a [¹⁸F]-fluoro-2-deoxy-D-glucose PET/CT study. *Crit Care Med* 37:2216–2222
19. Bellani G, Guerra L, Musch G et al (2011) Lung regional metabolic activity and gas volume changes induced by tidal ventilation in patients with acute lung injury. *Am J Respir Crit Care Med* 183:1193
20. de Geus-Oei L-F, Visser EP, Krabbe PF et al (2006) Comparison of image-derived and arterial input functions for estimating the rate of glucose metabolism in therapy-monitoring 18F-FDG PET studies. *J Nucl Med* 47:945–949
21. Cobelli C, Saccomani MP, Ferrannini E et al (1989) A compartmental model to quantitate in vivo glucose transport in the human forearm. *Am J Physiol Endocrinol Metab* 257:E943–E958
22. Veronese M, Bertoldo A, Bishu S et al (2010) A spectral analysis approach for determination of regional rates of cerebral protein synthesis with the L-[¹⁵C]-leucine PET method. *J Cereb Blood Flow Metab* 30:1460–1476
23. Patlak CS, Blasberg RG, Fenstermacher JD (1983) Graphical evaluation of blood-to-brain transfer constants from multiple-time uptake data. *J Cereb Blood Flow Metab* 3:1–7
24. Chen DL, Mintun MA, Schuster DP (2004) Comparison of methods to quantitate 18F-FDG uptake with PET during experimental acute lung injury. *J Nucl Med* 45:1583–1590
25. Huang S-C (2000) Anatomy of SUV. *Nucl Med Biol* 27:643–646
26. MacQueen J (1967) Some methods for classification and analysis of multivariate observations [abstract]. 1: 14P
27. Bertoldo A, Vicini P, Sambucetti G et al (1998) Evaluation of compartmental and spectral analysis models of [¹⁸F] FDG kinetics for heart and brain studies with PET. *IEEE Trans Biomed Eng* 45:1429–1448
28. Cunningham VJ, Jones T (1993) Spectral analysis of dynamic PET studies. *J Cereb Blood Flow Metab* 13:15–23
29. Turkheimer F, Moresco R, Lucignani G et al (1994) The use of spectral analysis to determine regional cerebral glucose utilization with positron emission tomography and [¹⁸F] fluorodeoxyglucose: theory, implementation, and optimization procedures. *J Cereb Blood Flow Metab* 14:406–422
30. Veronese M, Schmidt KC, Smith CB, Bertoldo A (2012) Use of spectral analysis with iterative filter for voxelwise determination of regional rates of cerebral protein synthesis with L-[¹⁵C]-leucine PET. *J Cereb Blood Flow Metab* 32:1073–1085
31. Veronese M, Rizzo G, Turkheimer FE, Bertoldo A (2013) SAKE: a new quantification tool for positron emission tomography studies. *Comput Methods Programs Biomed* 111:199–213
32. van den Hoff J, Oehme L, Schramm G et al (2013) The PET-derived tumor-to-blood standard uptake ratio (SUR) is superior to tumor SUV as a surrogate parameter of the metabolic rate of FDG. *EJNMMI Res* 3:77
33. Veronese M, Rizzo G, Aboagye E, Bertoldo A (2014) Parametric imaging of 18F-fluoro-3-deoxy-3-l-fluorothymidine PET data to investigate tumour heterogeneity. *Eur J Nucl Med Mol Imaging* 41(9):1–12
34. Sokoloff L (1977) Relation between physiological function and energy metabolism in the central nervous system. *J Neurochem* 29:13–26
35. Jadvar H, Parker JA (2005) *Clinical PET and PET/CT*. Springer, New York
36. Chen DL, Richard J-C, Schuster DP (2004) Molecular imaging of enzyme function in lungs. In: Conn PM (ed) *Methods in enzymology*. Academic Press, New York, pp 315–333
37. Wienhard K, Schmand M, Casey ME et al (2002) The ECAT HRRT: performance and first clinical application of the new high resolution research tomograph. *IEEE Trans Nucl Sci* 49:104–110